Astron. Astrophys. 331, 428–438 (1998)

ASTRONOMY AND ASTROPHYSICS

The radio continuum halo of NGC 5775

N. Duric[1], **J. Irwin**[2], **and H. Bloemen**[3,4]

[1] Institute for Astrophysics, University of New Mexico, Albuquerque, NM 87131, USA
[2] Department of Physics, Stirling Hall, Queen's University, Kingston, Ont. K7L 3N6, Canada
[3] SRON-Utrecht, Sorbonnelaan 2, 3584 CA Utrecht, The Netherlands
[4] Leiden Observatory, P.O. Box 9513, 2300 RA Leiden, The Netherlands

Received 18 November 1996 / Accepted 15 September 1997

Abstract. Sensitive, scaled-array VLA radio-continuum observations of the edge-on galaxy NGC 5775, at 6 and 20 cm, show evidence of a radio-continuum halo that is detected up to 10–15 kpc above and below the plane. In addition, the presence of a radio continuum bridge connecting NGC 5775 to neighbouring NGC 5774 is confirmed, lending further support to reports that these galaxies form an interacting pair.

Detailed analysis of the radio continuum halo of NGC 5775 indicates that it is characterized by a relatively steep spectrum with a spectral index of $\approx$ 1.0. The spectral index of the disk is significantly flatter, averaging $\approx$ 0.6. To first order, there is no evidence for large-scale spectral changes as a function of distance from the mid-plane in either component. The superposition of the disk and halo components, with distinctly different spectral indices, accounts for the apparent spectral steepening of the observed (total) emission with distance from the mid-plane.

The spectral results presented here are consistent with the findings for NGC 3556 (Bloemen et al. 1993), which could be studied with a 2-3 times better linear resolution. As with NGC 3556 the relatively flat spectrum of the disk of NGC 5775 appears to be the result of an ensemble of discrete sources, embedded in diffuse steep-spectrum emission as found in the halo. It appears that the gradual spectral steepening away from the mid-plane found in previous studies of edge-on galaxies may be attributed to insufficient angular resolution, supplemented by the missing-flux problem.

In contrast to the absence of global spectral changes in the disk and halo there are localized features of flatter spectral index that appear to connect the disk to the halo. These "tentacles" of flatter spectral index are roughly vertical and may represent chimneys of localized convection.

Key words: cosmic rays – halos – radio continuum – galaxies

1. Introduction

It is now firmly established that some disk galaxies possess radio continuum halos. Since the primary form of emission in such halos is synchrotron radiation it follows that the disks of these galaxies are surrounded by cosmic rays and magnetic fields. Understanding the origin of the CR halos is critical to our understanding not only of CR propagation and origin but also of the niche halos fill in the evolution of galaxies. The link between halo constituents and phenomena in the disk, for example, provides valuable insight into how the evolution of the disk leads to the formation of halos. Detailed studies of the halos are important in their own right because of the potential to understand the distribution of matter within halos.

Radio continuum halos were discovered and studied through observations of galaxies oriented edge-on to our line of sight. Examples include NGC 253 (Carilli et al, 1992), NGC 891 (Allen et al, 1978; Hummel et al, 1991), NGC 4631 (Ekers & Sancisi, 1977; Hummel & Dettmar, 1990, Golla, 1993), NGC 4666 (Sukumar et al. 1988), M82 (Seaquist & Odegard, 1991; Reuter et al. 1995), NGC 3556 (Bloemen et al. 1993) and NGC 4666 (Dahlem et al. 1997). Typically, these studies have found that halos have steeper spectral indices than the disks and that there are, therefore, spectral gradients corresponding to the transition from the disk to the halo. Attempts have been made to model such gradients on the assumption that they result from energy losses of the CR electrons as they propagate from the disk into the halo. However, these studies were affected by inadequate resolution of the disk - halo interface, uncertainties in the thermal contribution to the radio emission (e.g. Golla, 1993) and missing flux in interferometric radio data.

Theoretical CR transport models utilizing diffusion, losses and convection have been developed and these now provide a basis for interpreting better quality radio continuum data (see for example, Ginzburg & Syrovatskii (1964), Lerche & Schlickeiser, 1982ab, Pohl & Schlickeiser. 1990ab and Bloemen, 1991 and references therein). These advances have led to the debate of whether CR halos are static (governed primarily by diffusion) or dynamical (governed primarily by convection). Attempts have been made to link both processes to events in the disks of galaxies but these have been largely inconclusive, again because of inadequate spatial resolution. The question of whether dynamical interactions with nearby companion galaxies affect the formation of halos has also been raised but the results remain in-

conclusive. Although NGC 4631 has a nearby companion, M82 has only a distant companion and NGC 891 apparently has none.

Much work has been invested in identifying vertical structures linking disks to their halos, the most dramatic results being the HI superbubbles observed in our own Galaxy (Heiles 1979, 1984) and other edge-on systems (Irwin & Seaquist 1990, Rand & van der Hulst 1993, Irwin 1994). These have also been seen in the geometry of the magnetic fields (Golla & Beck, 1991). The concepts of chimneys (Norman & Ikeuchi 1989) and fountains (Shapiro & Field 1976, Bregman 1980) were thus born (see also Stephens 1991 & Mirabel 1982). In the observational studies the biggest handicap has been the absence of sufficient resolution to either identify all but the largest (scales of a few kpc) vertical structures or resolve the disk-halo interface. At the same time it has been difficult to map all spatial structures corresponding to the halos because of the large angular sizes of the galaxies involved. This has also led to problems of missing flux and uncertainties in the determination of spectral index distributions as alluded to above. An important exception to this trend has been the work of Golla & Hummel (1994) who studied NGC 4631 at a linear resolution of $\approx$ 300 pc and avoided most of the above mentioned problems.

In an effort to further improve on the overall situation, we have begun a program of examining a sample of edge-on galaxies for which it is possible to study both the fine structure (on scales of a few hundred parsecs) and large structures (scales up to 25 kpc) simultaneously. Galaxies for which this is possible have to satisfy the multiple criteria of (i) being sufficiently edge-on, (ii) being close enough to allow good linear resolution with the VLA and (iii) be sufficiently small in angular extent to allow detection of large scale structure (thereby avoiding the missing flux conundrum). The 4 galaxies we chose for this study and which satisfy the above criteria are NGC 3556, NGC 5775, NGC 4517 and NGC 2683. In the case of NGC 3556 and NGC 5775 we have found evidence for large scale radio continuum halos. A preliminary report on the halo in NGC 3556 is found in Bloemen et al. (1993) where it is suggested that no large scale (kpc) disk-halo interface exists and that spectral index gradients are primarily artifacts of beam smearing (a similar suggestion was made by Allen et al. (1979) for NGC 891).

The principal aim of this paper is to report the discovery of an extensive halo around NGC 5775 and confirm the existence of a radio continuum bridge linking NGC 5775 to its interacting companion, NGC 5774 (Sect. 2). In a follow-up paper we will model the propagation of CR electrons out of the disk in terms of diffusion and loss processes.

2. Data acquisition and analysis

2.1. The observations

The radio continuum observations, discussed in this paper, were taken over a span of several years utilizing 2 observing frequencies and a number of VLA[1] configurations. The C band(6 cm) data were collected in the C, D and C/D hybrid arrays for a total observing time of 6 hours. Data at L band (20 cm) were taken in the B, C and D arrays for a total of 8 hours. The resulting uv coverage at L band matches that at C band and in addition has sensitivity to the larger angular scales between $300''$ and $900''$. The sensitivity to the larger structures is illustrated in Fig. 1a which shows a low-resolution 20 cm map of the interacting pair. The extensive halo and bridge connecting NGC 5775 to the neighboring galaxy NGC 5774 are evident. A high resolution 20 cm map is shown in Fig. 1b. The detailed structure of the disk and inner halo are evident at the resolution of $5''$ or 600 pc.

The uv data from the various arrays were combined in a weighted manner with the weights determined by the sum of gridding weights determined in the AIPS program MX. The data sets were self-calibrated to correct phase errors and to increase the dynamic range. The maps used for most of the analysis were restored with a synthesized beam of $15'' \times 13''$. At the distance of NGC 5775 (24.8 Mpc) the beam corresponds to an area of 1.8×1.6 kpc. The rms noise was 25 μJy/beam at both the C and L bands. The latter is confusion limited. At this resolution there was no evidence for missing flux at either frequency. The dynamic range in these maps is $\approx$ 300. The combined 20 cm map is shown in Fig. 2a and the 6 cm map in 2b. The spectral index map obtained from these images is shown in 2c.

2.2. Properties of the radio continuum emission

The radio continuum maps show significant extensions out of the plane of NGC 5775. At the assumed distance of 24.8 Mpc the outermost contours of emission at 20 cm (Fig. 1a) extend to 15 kpc above and below the plane, well beyond the HI distribution. There is also a radio continuum bridge connecting NGC 5775 and NGC 5774 (Irwin & Caron, 1994). The radio continuum disk of NGC 5775 is 37 kpc in extent making the halo-to-disk aspect ratio 0.8 at the outermost significant contour. The integrated flux densities of NGC 5775 (not including the bridge) were calculated using a technique similar to aperture photometry. This technique yielded flux densities of 96 ± 1 mJy at 6 cm and 248 ± 1 mJy at 20 cm. These flux densities are consistent with integrated flux densities published in the literature and with Effelsberg single dish data obtained independently by R. Beck and N. Duric. The resulting integrated spectral index is 0.78 ± 0.01.

We have searched for negative bowls and found only a very shallow one at 6 cm and 20 cm. In each case the DC level was depressed by less than half the rms noise of 25 μJy/beam. There was little systematic difference between the two bowls further minimizing the effect on the spectral index. Typical errors in the spectral index in the outer regions of the halo are $\approx \pm 0.1$. The small systematics arising from the bowls would only fractionally increase these uncertainties. The spectral index map

[1] The National Radio Astronomy Observatory is operated by Associated Universities Inc., under cooperative agreement with the National Science Foundation

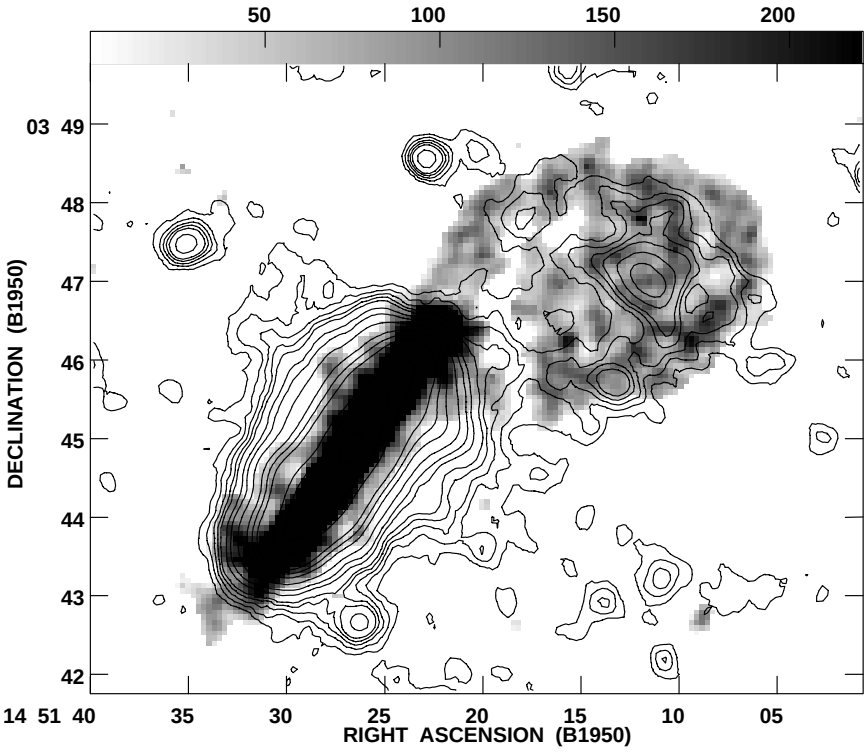

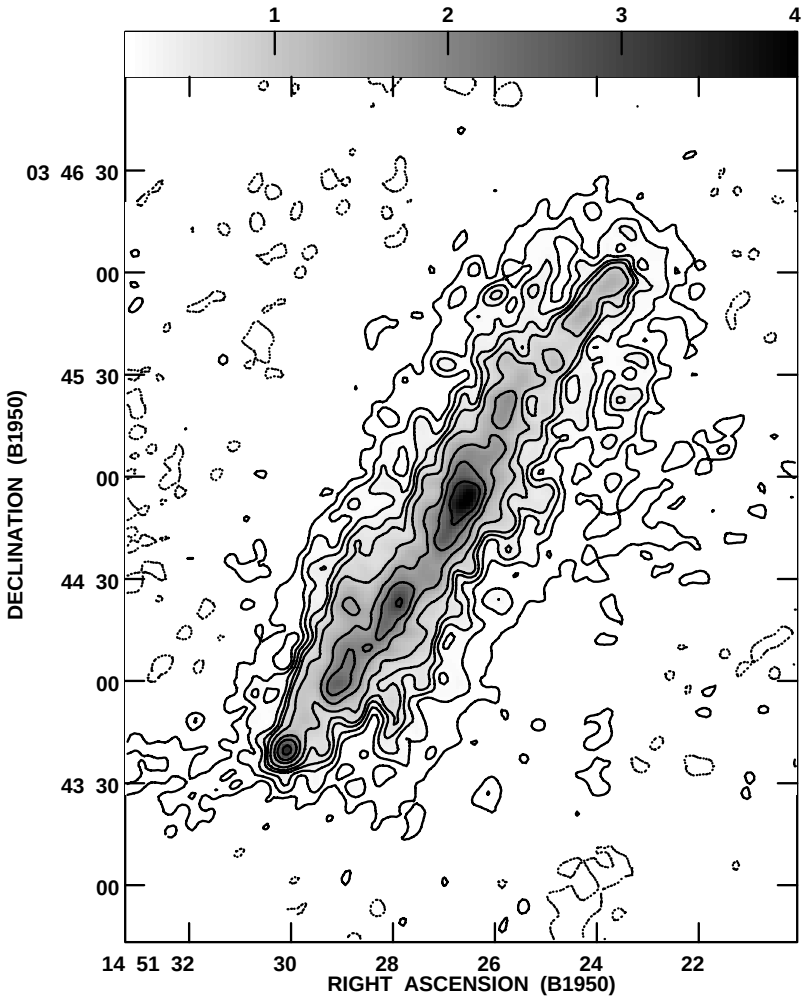

Fig. 1. a Low-resolution 20 cm contour map emphasizing the large scale radio continuum structure of NGC 5775 / NGC 5774. The continuum contours are superimposed on a grey-scale HI image to show the relationship between the synchrotron-emitting CR electrons and the neutral hydrogen gas. The continuum and HI images were restored with a 23.5″ beam and 13.5″ beam, respectively. The rms noise in the continuum map is 35 μJy/beam. The contours plotted represent flux densities of 2, 4, 6, 8, 10, 15, 20, 30, 50, 70, 100, 300, 500 and 1000 times 30 μJy/beam. The greyscale is in units of 10^{19} cm^{-2}. The HI gas is concentrated to the disk of NGC 5775 more so than the relativistic electrons although some low density HI appears to exist in the mid latitudes of the halo. **b** High-resolution 20 cm contour and grey-scale map of NGC 5775, restored with a 5″ beam, emphasizing the smaller-scale structure. The rms noise is 30 μJy/beam and the contours represent flux densities of -3, 3, 6, 10, 15, 20, 30, 50, 70 and 100 times 30 μJy/beam. The greyscale range is in mJy/beam for this and all following figures.

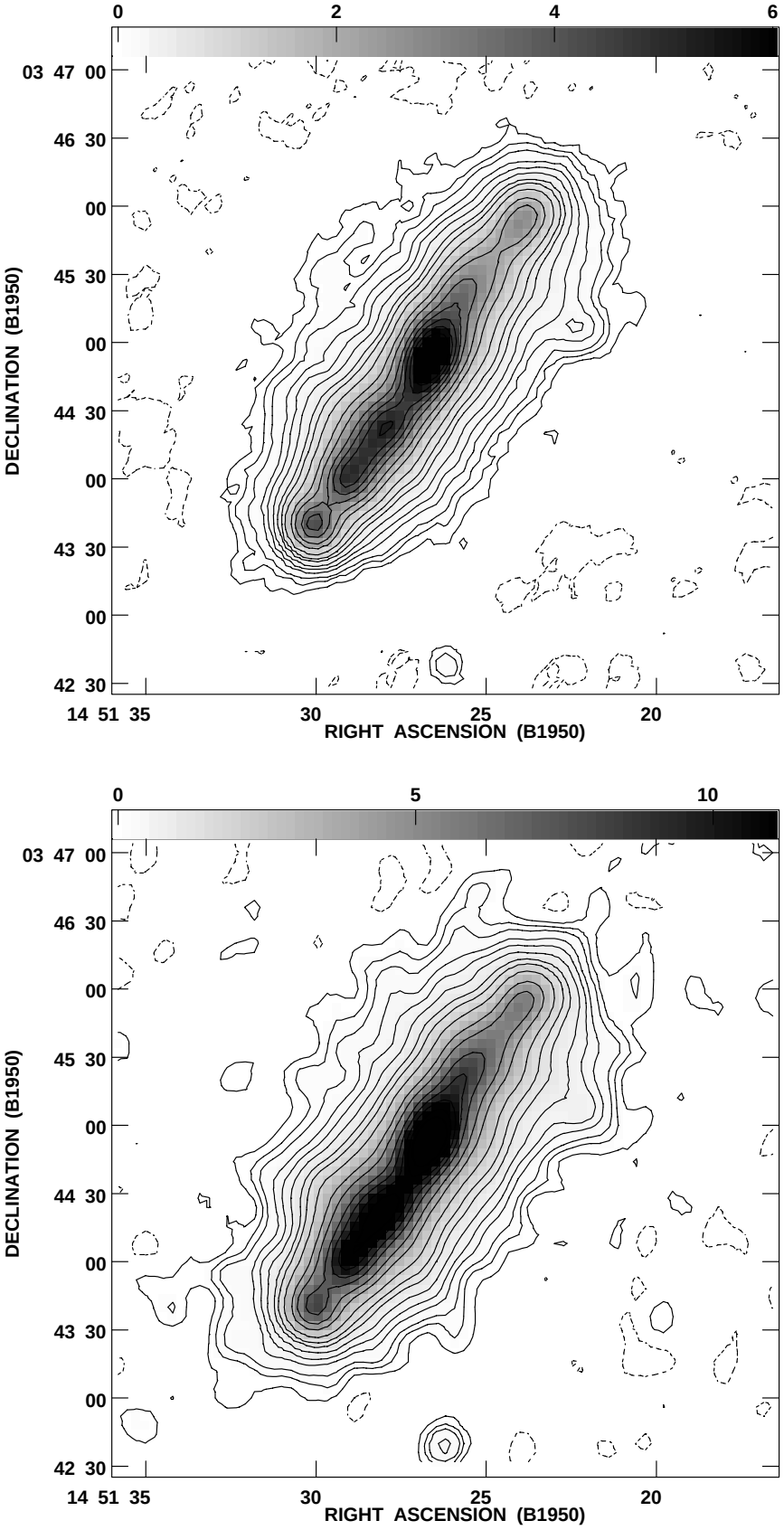

Fig. 2. a The 20 cm radio continuum image used in the analysis. With a restoring beam of $15'' \times 13''$, it represents the net result of combining the B, C and D array data. The rms noise in this map is 25 μJy/beam. The contours represent 1, 2, 3, 5, 7, 10, 15, 20, 30, 50, 70, 100, 125, 150, 175, 200, 300, 500, 750 and 1000 times 70 μJy/beam. **b** The 6 cm continuum image used in the analysis. With a restoring beam of $15'' \times 13''$, it represents net result of combining the C and D array data. The rms noise in this map is 25 μJy/beam. The contours represent 1, 2, 3, 5, 7, 10, 15, 20, 30, 50, 70, 100, 125, 150, 175 and 200 times 30 μJy/beam.

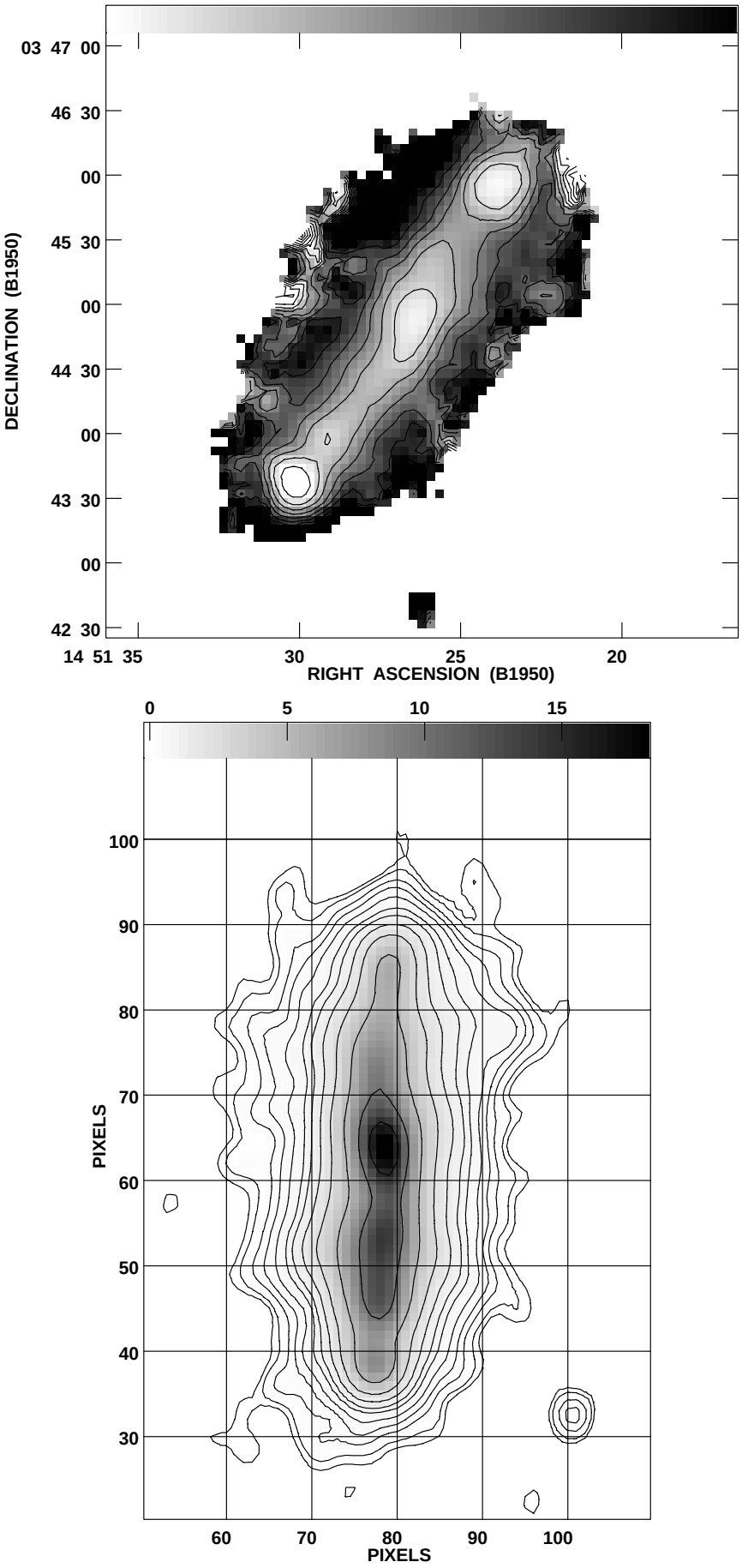

Fig. 2. c The spectral index map made by combining the maps from 2a and 2b. The spectral index, α, is defined according to the $S(\nu) \propto \nu^{-\alpha}$ convention. The index map was made after clipping the 20 cm and 6 cm maps at the 70 and 30 μJy/beam levels, respectively. The spectral index ranges from a low of 0.5 to a high of 1.2. The contours are presented in increments of 0.1, starting at 0.5 (white) and ending at 1.2 (black). Locally larger values are the result of combining pixels of low statistical significance. **d** The 20 cm image rotated to a vertical orientation. The grid lines represent pixel rows and columns referred to in the analysis. The horizontal rows are those along which the image slices were produced. The labeling scheme is that of the analysis referred to in the text.

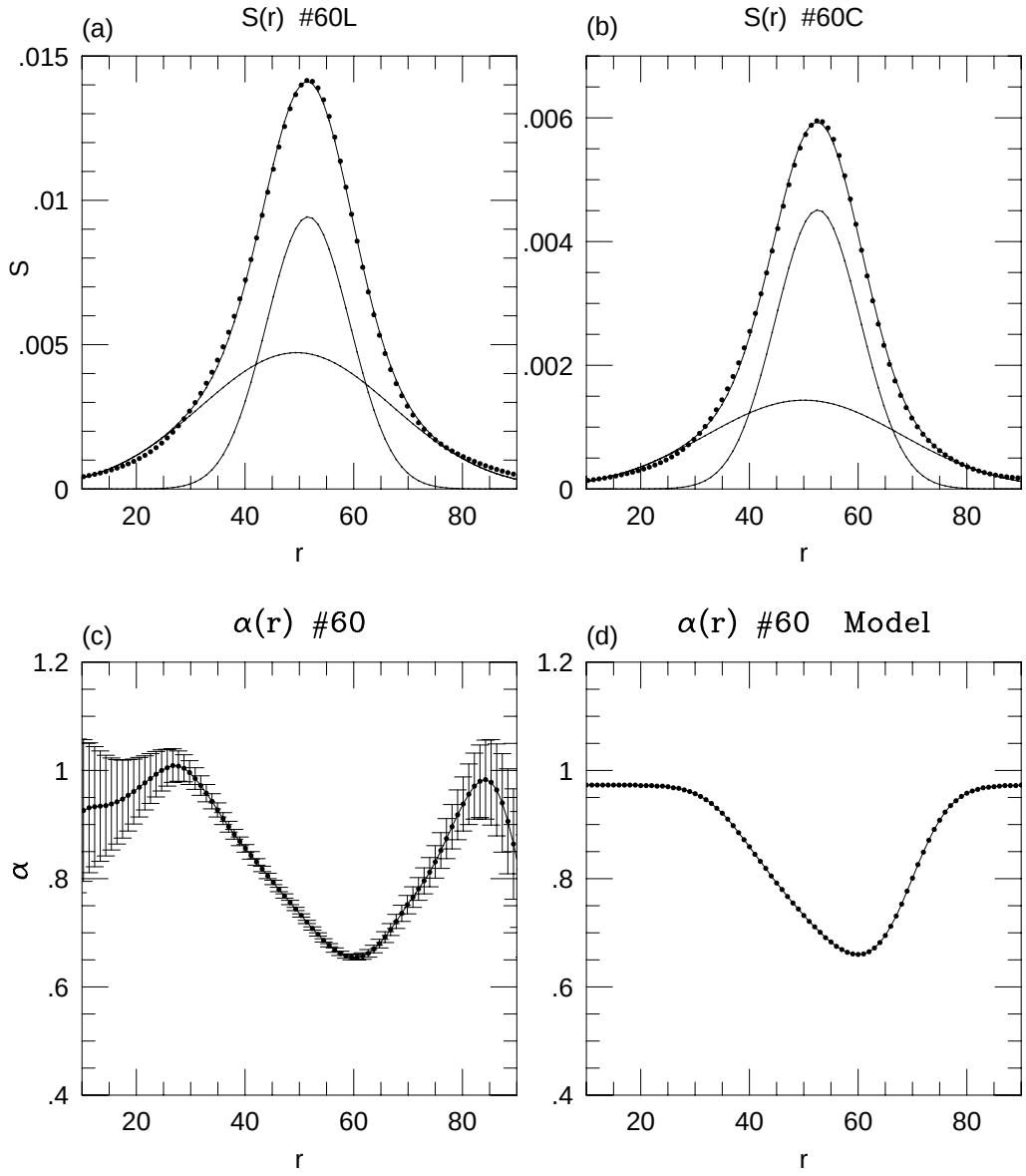

Fig. 3. a A sample image slice along row 60 from the 20 cm map (see Fig. 2d). The pixel values, in Janskys, are shown as solid dots. The horizontal axis is in seconds of arc. Each slice in this analysis was 100 pixels or 350″ long, centered roughly on the major axis of NGC 5775. The solid curve passing through the points is the best fit sum of 2 gaussians. The gaussian components are shown individually under the slice. We identify the narrow, higher gaussian as the disk and the broader, lower gaussian as the halo. **b** The same as in 3a but at 6 cm. **c** The observed spectral index profile obtained by combining the 2 slices from 3a and 3b. The error bars were calculated by propagating the rms errors from the 20 cm and 6 cm maps through the spectral index calculations. **d** A synthesized spectral index profile for slice # 60, made by combining a disk component with α = 0.6 and a halo component with α = 1.0 and offsetting them slightly by an amount obtained from the fits in 3a and 3b.

(Fig. 2c) indicates that the disk is characterized by a spectral index varying from 0.6 to 0.7 while the emission outside the disk steepens to 0.9 - 1.1.

The radio continuum bridge is undetected at 6 cm so that its spectral index is not known. Assuming the same index as the halo ($\approx$ 1.0) leads to estimates similar to those in the outer halo.

2.3. Disk and halo decomposition

In an earlier study of NGC 3556 (Bleomen, Duric and Irwin, 1993) we found that the disk and halo were distinct components, each characterized by a relatively constant spectral index. No evidence was found for a global spectral index gradient within the radio continuum halo of NGC 3556 to a linear resolution of 200 pc. Motivated by these findings we undertook a quantitative analysis of the disk and halo of NGC 5775 by analysing the radio continuum and spectral index profiles perpendicular to the plane of NGC 5775.

Profiles of emission at each frequency were determined using image slices parallel to the minor axis. The galaxy image was rotated in AIPS so that slices parallel to the minor axis (as

Table 1. NGC 5775 - Properties of the disk and halo

#	R_{20}^D	R_{20}^H	R_6^D	R_6^H	σ_{20}^D	σ_{20}^H	σ_6^D	σ_6^H	S_{20}^D	S_{20}^H	S_6^D	S_6^H	α_D	α_H
35	47.4	40.7	48.6	42.3	20.2	57.0	17.6	46.1	2.1	0.5	0.9	0.2	0.71	0.73
40	46.7	47.5	46.7	48.6	16.9	40.0	16.7	38.8	5.8	2.3	3.0	0.7	0.54	0.97
45	48.2	48.7	48.5	49.8	19.2	42.0	18.5	46.6	8.8	2.8	4.1	0.8	0.63	1.04
50	48.7	47.4	49.3	48.3	20.2	44.8	19.9	46.3	8.3	5.0	3.7	1.4	0.67	1.05
55	51.0	47.6	51.0	49.1	18.3	39.7	18.8	41.9	7.6	6.1	3.6	1.7	0.6	1.10
60	51.6	49.5	52.6	50.1	18.0	41.4	18.4	42.4	9.4	4.7	4.5	1.4	0.60	0.98
65	50.1	51.2	50.5	51.6	18.4	42.7	18.8	46.6	13.8	4.6	7.1	1.2	0.54	1.08
70	48.3	52.0	48.6	53.7	20.1	46.1	20.1	45.9	7.2	3.3	3.3	1.1	0.65	0.91
75	48.4	52.9	48.5	55.5	22.5	61.5	21.9	61.2	6.4	1.9	2.7	0.5	0.71	1.01
80	50.2	53.6	50.3	54.1	20.1	62.4	20.4	61.3	4.3	1.6	1.8	0.5	0.72	1.02
85	52.5	54.3	52.5	55.4	16.3	53.0	17.3	59.0	4.7	1.4	2.4	0.4	0.54	1.10

determined from HI dynamical models, see Irwin, 1994) could be produced by simply reading off image rows. Fig. 2d displays the geometry used. The cuts were generated in AIPS using the SLICE set of routines. Slices were generated from image rows spaced 3.5″ apart starting with row # 35 and ending with #85 (see Fig. 2d). Each slice consists of 100 columns or 350″ centered roughly on the major axis of NGC 5775. Sample profiles, corresponding to slice # 60, are shown in Fig. 3a (20 cm) and 3b (6 cm). The corresponding spectral index profile is shown in Fig. 3c. We attempted to fit gaussians to the emission profiles. Gaussians were chosen for computational convenience and the final results did not depend on this particular choice of the fitting function. None of the profiles could be adequately fit with a single gaussian. However, fitting 2 gaussians was very successful as shown in Fig. 3a and 3b. The fit was sufficiently accurate that we were able to estimate the underlying halo profile even at the origin (z = 0, corresponding to a line of sight passing through the disk).

To test the consistency of the fits we left the peak flux density, width and position of the gaussians as free parameters. The results are summarized in Table 1. The quoted widths are full widths at half power and they have not been deconvolved from the beam. The deconvolved widths are listed in Table 2 and are obtained simply by taking $\sigma = \sqrt{\sigma_0^2 - \sigma_b^2}$, where σ_b = 13.5″, is the beam width in the direction of the minor axis and σ_0 is the quoted width in Table 1. The peak positions of the disk and halo profiles are always found to be coincident to within a fraction of the beam width arguing for a true superposition of gaussians. The widths were consistent for both components regardless of where the cuts were taken (except toward the edges of the disk where the projected halo emission narrows) and most importantly, *similar widths were obtained for the 6 and 20 cm halo profiles and for the 6 and 20 cm disk profiles*.

2.3.1. Explanation of Table 1

Column 1. Slice number. Numbers increase toward the NW (up in Fig. 2d).
Column 2. Position of centre of disk component at 20 cm. The position is relative to the beginning of the slice in units of seconds of arc.
Column 3. Position of halo component at 20 cm.
Column 4. Position of disk component at 6 cm.
Column 5. Position of halo component at 6 cm.
Column 6. Half-Power Full-Width of disk component at 20 cm in seconds of arc.
Column 7. Half-Power Full Width of halo component at 20 cm.
Column 8. Half-Power Full Width of disk component at 6 cm.
Column 9. Half-Power Full Width of halo component at 6 cm.
Column 10. Peak flux density of disk component at 20 cm in mJy/beam.
Column 11. Peak flux density of halo component at 20 cm.
Column 12. Peak flux density of disk component at 6 cm.
Column 13. Peak flux density of halo component at 6 cm.
Column 14. Spectral index of disk component at z = 0.
Column 15. Spectral index of halo component at z = 0.

2.3.2. Explanation of Table 2

Column 1. Slice number. Numbers increase toward the NW (up).
Column 2. Half-Power Full-Width of disk component at 20 cm in seconds of arc.
Column 3. Half-Power Full Width of halo component at 20 cm.
Column 4. Half-Power Full Width of disk component at 6 cm in seconds of arc.
Column 5. Half-Power Full Width of halo component at 6 cm.
Column 6. The gaussian $1/e$ scale height of disk at 20 cm (kpc).
Column 7. The gaussian $1/e$ scale height of halo at 20 cm.
Column 8. The gaussian $1/e$ scale height of disk at 6 cm.
Column 9. The gaussian $1/e$ scale height of halo at 6 cm.

2.3.3. Properties of the disk and halo

Typically, the disk was found to have a half-power, full-width of $16'' - 21''$. After beam deconvolution this yields a range of $8.5'' - 16''$ or 1.0 - 2.0 kpc. The gaussian $1/e$ scale height is therefore 0.7 - 1.4 kpc. The disk is probably thinner than this since the galaxy is not viewed completely edge-on (i = 87^o, Irwin 1994). However, given the beam size of $15'' \times 13''$ (1.8 $\times$ 1.6 kpc $\approx 37 kpc \cos(i)$), the above numbers are sufficiently accurate for our purposes. The $1/e$ scale heights obtained for the halo range from 2.8 to 4.7 kpc (Table 1). The decomposition of the emission into disk and halo components allowed us

Table 2. NGC 5775 - deconvolved halo and disk parameters

#	σ_{20}^{D}	σ_{20}^{H}	σ_{6}^{D}	σ_{6}^{H}	h_{20}^{D}	h_{20}^{H}	h_{6}^{D}	h_{6}^{H}
35	15.0	55.4	11.3	44.1	1.2	4.3	0.9	3.4
40	10.2	37.8	9.8	36.4	0.8	2.9	0.8	2.8
45	13.7	39.8	12.6	44.6	1.1	3.1	1.0	3.4
50	15.0	42.7	14.6	44.3	1.2	3.3	1.1	3.4
55	12.4	37.3	13.1	39.7	1.0	2.9	1.0	3.1
60	11.9	39.1	12.5	40.2	0.9	3.0	1.0	3.1
65	12.5	40.5	13.1	44.6	1.0	3.1	1.0	3.4
70	14.9	44.1	14.9	43.9	1.1	3.4	1.1	3.4
75	18.0	60.0	17.2	59.7	1.4	4.6	1.3	4.6
80	14.9	60.9	15.3	59.8	1.1	4.7	1.2	4.6
85	9.1	51.3	10.8	57.4	0.7	3.9	0.8	4.4

to estimate the flux densities of the two components separately. The peak flux densities at 6 and 20 cm for the various slices are listed in Table 1. Also listed are the resulting spectral indices. It appears that the halo and disk spectral indices are relatively independent of where the slices are taken. Furthermore, the similarity of the profile widths at 6 and 20 cm also suggests that *the spectral indices of the halo and disk are relatively constant with distance from the plane* which leads us to propose that the the radio continuum distribution of NGC 5775 is a superposition of a disk and halo component each with a *constant* spectral index (no spectral index gradients). The consequences of such a model are discussed in Sect. 2.3.5.

The spectral indices of the disk and halo are listed in Table 1 for $z = 0$. The disk index ranges from 0.54 to 0.72 while the halo index ranges from 0.91 to 1.13. It follows that the spectral index of the differential electron spectrum ($\gamma = 2\alpha - 1$) for the disk is in the range, $\gamma = 2.1 - 2.4$ and for the halo, $\gamma = 2.8 - 3.2$.

Fig. 3d illustrates the spectral index profile obtained by adding 2 gaussians (disk and halo) at each frequency and dividing the resulting 6 cm and 20 cm profiles. The halo and disk gaussians are each taken to have frequency independent widths and the disk and gaussian components are displaced by the amounts indicated in Table 1. In this example, taken from the fits to slice # 60, the disk component has a constant spectral index (independent of z) of 0.6 while the halo component has a fixed index of 1.0. The superposition of the 2 components qualitatively reproduces the radio continuum profile and shows an *apparent* spectral index gradient. The spectral index gradient produced by the superposition occurs on a scale not much larger than the beam (after beam convolution it is less than 2 beam widths in extent). Given that the gradient is a projection effect associated with line of sight addition of the 2 components it is of interest to ask whether there is any need for a disk-halo interface at all, from a physical point of view.

2.3.4. High-resolution analysis

Unfortunately, the above analysis could not be performed at the higher resolution, such as that shown in Fig. 1b. The signal to noise per beam is inadequate for studying the outer halo. However, given the sensitivity to much smaller scales ($5'' = 600$ pc), the high-resolution data are well suited for analysing the properties of the disk and inner halo. To optimize the signal to noise ratio, we produced integrated profiles, as shown in Fig. 4. The left column represents emission integrated along rows parallel to the major axis. The resulting minor axis profile has the full $5''$ resolution along the minor axis where each point on the profile represents all the flux density at that distance from the plane. The bar in the top left figure represents 1 kpc at the assumed distance of 25 kpc. The top left figure shows the average 6 cm flux density in units of Jy/beam plotted as a function of distance (in arcseconds). The middle left figure shows the same type of profile for the 20 cm emission. The bottom left figure shows the spectral index distribution corresponding to the 6 cm and 20 cm profiles. The right column shows the major axis profiles using slices along the major axis that are only $1''$ wide. The top left figure shows the 6 cm profile, the middle figure shows the 20 cm profile and the bottom figure shows the spectral index distributions.

It is evident that the minor axis profile shows a narrow component corresponding to the disk and a broader component corresponding to the halo. The spectral index profile was formed by including only those points for which the 6 cm and 20 cm flux densities exceed a level 3 times the rms noise at each frequency. Thus, the spectral index profile does not extend across the full range of the flux density profiles. Nevertheless, the spectral profile extends into the inner halo and demonstrates the distinct separation of the disk and halo spectral indices. As the bottom left profile in Fig. 4 indicates the spectral index changes abruptly from a value of about 0.6 to values exceeding 0.8 over an angular distance of $\approx 15''$, about 3 beams. These figures represent the maximum possible gradient because the galaxy is not exactly edge-on and some of the apparent gradient may be the result of the integration used to produce the profile.

The slice along the major axis is only $1''$ wide. The spectral index profile therefore exhibits strong variation along the slice. As expected, relatively bright disk sources have flatter spectra ($\approx 0.5 - 0.7$). However, there are regions in the disk with indices approaching 0.95. Such steep spectrum regions are sometimes seen in the plane of our own Galaxy (Reich & Reich, 1988) although in the latter case it is difficult to compare with halo data because of the unfavorable perspective of the observer. The steep-spectrum emission tends to be fainter and is associated with inter-source regions. Furthermore, the steep-

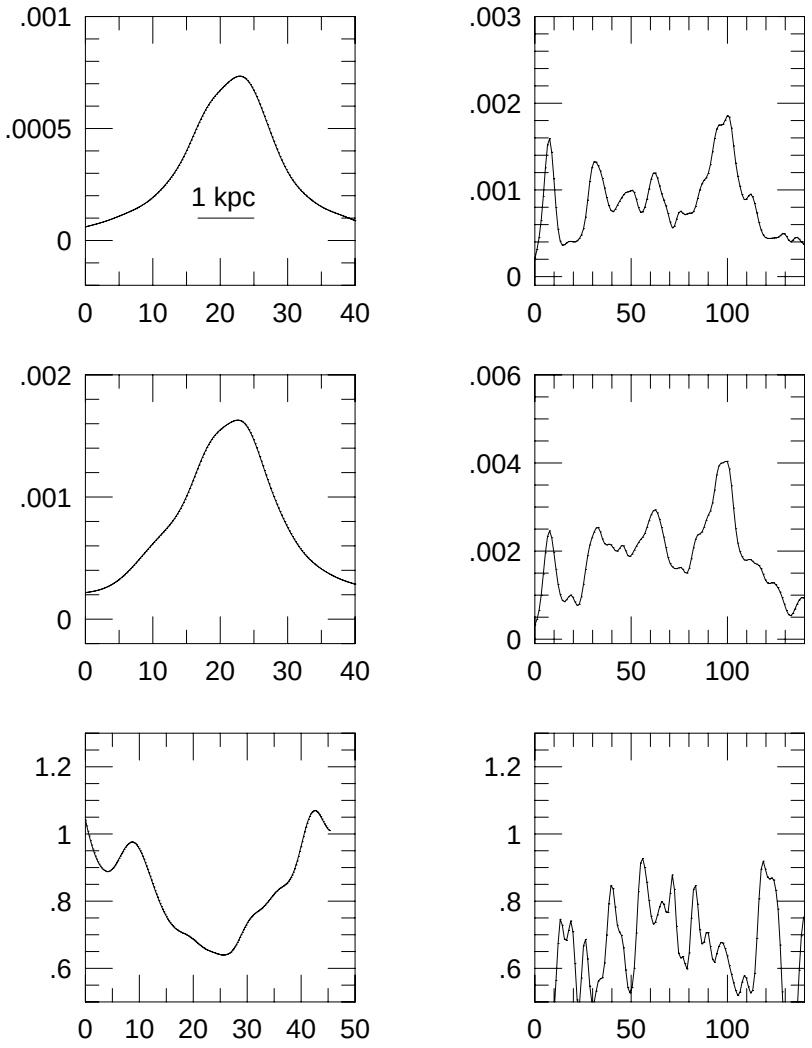

Fig. 4. Profiles of 6 cm, 20 cm and spectral index variation from our high-resolution maps, along the major and minor axes. To optimize the signal to noise, we produced integrated profiles. The left column represents emission integrated along rows, 140″ long, parallel to the major axis. The resulting minor axis profile has the full 5″ resolution along the minor axis where each point on the profile represents all the flux density at that distance from the plane. The bar in the top left figure represents 1 kpc at the assumed distance of 25 kpc. The top left figure shows the average 6 cm flux density in units of Jy/beam plotted as a function of distance (in arcseconds). The middle left figure shows the same type of profile for the 20 cm emission. The bottom left figure shows the spectral index distribution corresponding to the 6 cm and 20 cm profiles. The right column shows the major axis profiles (140″ long) from slices along the major axis that are only 1″ wide. The top right figure shows the 6 cm profile, the middle figure shows the 20 cm profile and the bottom figure shows the spectral index distribution.

spectrum inter-source regions in the disk have spectral indices characteristic of the inner halo. Thus, it is conceivable that the inter-source disk emission is actually associated with the halo component, ie flat spectrum discrete sources in the disk are embedded in a large, steep spectrum halo that both permeates the disk and extends far from it. This finding is consistent with those we previously reported for NGC 3556 (Bloemen et al. 1993).

2.3.5. Implications of the 2-component disk-halo model

One consequence of our results is the implication that the CR electrons lose much of their energy close to or within the discrete regions that we identified earlier as possible star forming complexes (discrete at the level of our linear resolution of 600 pc) whereas in the intersource regions (low-density regions of the disk and halo) the relativistic electrons lose energy at a much slower rate. In the case of synchrotron and/or inverse Compton losses the spectral index steepens abruptly by 0.5. To determine if such behavior is physically reasonable we performed a straightforward analysis of CR electron propagation.

According to CR transport theory, relativistic electrons propagate at or near the Alfven velocity in any frame in which they are fully scattered and in which they establish an isotropic distribution (e.g. Wentzel, 1974). The Alfven velocity is given by

$$V_A = \frac{B}{\sqrt{4\pi\rho_i}} \tag{1}$$

where ρ_i is the density of the ionized medium through which the electrons are propagating and B is the strength of the ambient magnetic field.

As the electrons propagate, they lose energy through synchrotron radiation and through interactions with ambient photons, through the Inverse Compton process. Taking the total energy density of the magnetic field and ambient photons,

$$U_T = \frac{B^2}{8\pi} + U_*$$

the energy loss time scale for electrons is then

$$\tau_e = 3 \times 10^8 \left[\frac{U_T}{\mathrm{eV\,cm^{-3}}} \; \frac{E}{\mathrm{GeV}} \right]^{-1} \tag{2}$$

where E is the kinetic energy of the electron (e.g. Duric, 1991).

By combining Eqs. (1) and (2) it is possible to define the propagation scale length. The photon energy densities are difficult to estimate in NGC 5775. However, the result is not strongly dependent on them and we therefore proceed by ignoring the photon contribution to the losses. Combining Eqs. (1) and (2),

$$d \approx V_A \tau_e = 23 \left[\frac{\sqrt{n_i}}{\mathrm{cm}^{-3}} \; \frac{B}{\mu\mathrm{G}} \; \frac{E}{\mathrm{GeV}} \right]^{-1} \mathrm{kpc}. \qquad (3)$$

In our own Galaxy the intercloud medium (the presumed equivalent of the intersource medium in NGC 5775) is characterized with $n_i \approx 0.02$ (Taylor & Cordes, 1997) while the star forming regions tend to be much denser with $n_i \approx 1$. We have adopted these values for the intersource and discrete regions in NGC 5775 respectively since we have no data on the ionized gas densities. That such distinct ionized regions exist in other galaxies is demonstrated very clearly by the example of NGC 3079 (Veilleux et al, 1995). In the case of the magnetic fields we were able to estimate them using equipartition calculations. For typical hot spots in the disk (see Fig. 1b) we estimate $B \approx 10\mu G$ while for the intersource region we obtain $B \approx 3\mu G$, assuming a filling factor of 1 and a cosmic ray proton to electron ratio of 40. The characteristic energies of electrons radiating at 1.4 GHz are 8 GeV and 13 GeV respectively.

Substituting the above parameters into Eq. (3) yields characteristic propagation distances of 0.3 kpc and 4.2 kpc for the source and intersource regions respectively. These numbers appear to support our contention that CR electrons lose most of their energy close to their sources. The above propagation scale length of 0.3 kpc is consistent with the upper limits of ≈ 600 pc for the sizes of the discrete sources in the disk of NGC 5775. Outside the source regions the electrons can propagate much faster and at the same time lose energy more slowly because of the lower B fields and photon densities in the intercloud regions. (The inclusion of photon energy densities in the above discussion would have increased the difference between the two propagation scale lengths thereby strengthening our conclusions.) Once in the intersource region the CR electrons can propagate many kiloparsecs before losing significant energy. By that point they have most likely populated the halo where the lower densities and magnetic field strengths increase the propagation scale lengths even further. We therefore conclude that it is quite plausible for the halo to be characterized by a relatively constant spectral index distribution and for the disk to be characterized by a diffuse disk component, indistinguishable from the halo, as well as a component consisting of discrete sources.

The above findings have additional implications regarding the interpretation of radio continuum emission of galaxies. According to our picture, discrete sources of emission play an important role in determining the global properties of the CR electrons. Furthermore, there exist two spectrally distinct disk components of radio emission. It is not, of course, clear that such a two-component disk model applies to other galaxies, it may only be associated with strong radio continuum halos. Nevertheless, it is interesting to speculate on the implications of a two-component disk model on equipartition calculations. To first order, the discrete sources that populate the disk are also the brightest and will, in general, dominate the integrated synchrotron emission of the disk. Thus, the primary effect is to introduce a filling factor for emission, ϕ that is significantly less than unity, contrary to the usual assumption. Since the minimum nonthermal energy, U_{min} scales as $\phi^{3/7}$ the major effect is to reduce the nonthermal energy. In the case of the magnetic field, $B \propto \phi^{-2/7}$ so that the estimate of the B field is increased. Our data do not allow an estimate of ϕ but we note that the above dependencies on ϕ are weak and we therefore anticipate that the above effects are modest. In any case, assuming a smaller ϕ leads to smaller propagation lengths thereby strengthening the above arguments.

Before these findings can be generalized to all galaxies, further high-resolution observations are needed of galaxies with and without halos.

2.3.6. Deviations from a 2-component disk-halo model

The spectral index map (Fig. 2c) shows structure, besides a general steepening from disk to halo, which cannot be reproduced by the superposition of two (disk+halo) gaussian components alone. This structure appears as "tentacles" of flatter spectral index which seem to connect specific positions in the disk to the upper halo. An example of these departures is also illustrated by slice 60. In the pure disk+halo model (Fig. 3d) the spectral index must remain constant at the value of the halo spectral index at very large scale heights, whereas the data (Fig. 3c) show a slight flattening of the index again at the largest distances from the plane. Thus, while a superposition of two (halo + disk) components matches the global observations very well, certain regions show a flatter spectral index well into the halo.

In the context of diffusion/convection models, maintaining a flatter spectral index to high latitude is often taken to be indicative of winds (e.g. Lerche & Schlickeiser, 1982ab) or a dynamical halo such as the one described by Pohl & Schlickeiser (1990). The morphology of these regions also resembles "channels". Thus these features are reminiscent of Chimneys as suggested by Norman & Ikeuchi (1989) and now observed in the Milky Way (Normandeau et al. 1996). It is interesting how obvious these features are in the spectral index map in comparison to the total intensity images (Fig. 2a, 2b). While radio continuum extensions can usually be identified with the spectral index channels, they are sometimes subtle. More detailed comparisons between the spectral index map and observations at other frequencies as well as details of the CR propagation will be described in future papers.

3. Conclusions

1. New scaled-array VLA radio-continuum observations of the edge-on galaxy NGC 5775 at 6 and 20 cm show evidence of a radio-continuum halo that is detected up to 10–15 kpc above and below the plane. A bridge connecting NGC 5775 to the neighbouring Galaxy NGC 5774 is confirmed, which lends further

support to reports that these galaxies form an interacting pair.

2. Slices through the 6 and 20 cm images parallel to the minor axis can be accurately described by the sum of two Gaussian components, the widths of which are remarkably similar at 6 and 20 cm. The broad (halo) component has a gaussian 1/e scale height of about 3.5 kpc. The narrow (disk) component has a scale height of about 1 kpc (after deconvolution). The actual scale height of the radio-continuum disk is probably smaller because the galaxy is not viewed completely edge-on.

3. In view of the similar scale heights at 6 and 20 cm, which holds for both the disk and halo components, there is, to a first order approximation, no indication of large-scale spectral changes as a function of distance from the mid-plane in the individual components. We conclude that there are no significant gradients on scales greater than $\approx$ 1 kpc. The spectral index α of the disk component ranges from about 0.55 to 0.7 for the different slices and that of the halo from about 0.9 to 1.1. It follows that the spectral index of the differential electron spectrum ($\gamma = 2\alpha - 1$) for the disk is in the range $\gamma = 2.1 - 2.4$ and for the halo $\gamma = 2.8 - 3.2$. The superposition of the disk and halo components, with distinctly different spectral indices, accounts for the apparent spectral steepening of the observed (total) emission with distance from the mid-plane.

4. The spectral results presented here are consistent with the findings for NGC 3556 (Bloemen et al. 1993), which could be studied with a 2–3 times better linear resolution. As with NGC 3556 the relatively flat spectrum of the disk of NGC 5775 appears to be the result of an ensemble of localized sources, embedded in diffuse steep-spectrum emission as found in the halo. It appears that the gradual spectral steepening away from the mid-plane found in previous studies of edge-on galaxies may be attributed to insufficient angular resolution, supplemented by the missing-flux problem.

5. Our findings suggest that CR electron energy spectra evolve rapidly close to the acceleration sites and much more slowly thereafter. Typical propagation distances of the CR electrons radiating at 1.4 GHz are $\approx$ 0.3 kpc in the bright localized regions of the disk (the presumed sites of acceleration) and $>$ 4 kpc elsewhere (the halo and the intersource regions of the disk).

6. In addition to a global representation of the radio continuum emission as the superposition of disk + halo components, several distinct regions of flatter spectral index are also observed. These appear as "channels" connecting the disk to the halo and may represent Chimneys as described by Norman & Ikeuchi (1989).

Acknowledgements. HB and ND acknowledge support through Grant # 0189/89 of the NATO Scientific Affairs Division.

References

Allen R.J., Baldwin J.E., Sancisi R. 1978, A&A 62, 397
de Bruyn A.G., Hummel E. 1979, A&A 73, 196
Bloemen 1991 in *The Interpretation of Modern Synthesis Observations of Spiral Galaxies*, eds N. Duric and P.C. Crane, ASP Conference Series 18, 27
Bloemen H., Duric N., Irwin J. 1993, Proc 23rd ICRC 2, 279
Bregman J. N. 1980, ApJ 236, 577.
Carilli C.L., Holdaway M.A., Ho P.T.P., de Pree C.G. 1992, ApJ 399, 59
Dahlem M., Petr M.G., Lehnert M.D., Heckman T.M., Ehle M. 1997, A&A 320, 731.
Duric N. 1991, in *The Interpretation of Modern Synthesis Observations of Spiral Galaxies*, eds. N. Duric and P.C. Crane, ASP Conference Series, Volume 18 p. 23.
Duric N., Bloemen H. 1990, Proc 21st ICRC 3, 217
Ekers R.D., Sancisi R. 1977, A&A 54, L973
Ginzburg V.L., Khazan Ya. M., Ptuskin V.S. 1980, Ap. Space Sci. 68, 295
Ginzburg V.L, Syrovatskii, S.I. 1964, "The Origin of Cosmic Rays", Pergamon Press, Oxford.
Golla G. 1993, *PhD Thesis*, University of Bonn
Golla G., Beck, R. 1991, in *The Interstellar Disk-Halo Connection in Galaxies*, ed. H. Bloemen, p. 275.
Golla G., Hummel E. 1994, A&A 284, 777.
Heiles C. 1979, ApJ 229, 533.
Heiles C. 1984, ApJS 55, 585.
Hummel E., Dahlem M., van der Hulst J.M., Sukumar, S. 1991, A&A 246,10
Hummel E., Dettmar R.J. 1990, A&A 236, 33.
Irwin J. A. 1994, ApJ 29, 618
Irwin J.A., Caron B.L. 1994, in *International Astrophysics Conference on Mass-Transfer Induced Activity in Galaxies* ed. I. Shlosman (Cambridge University Press), p362.
Irwin J. A., Seaquist E. R. 1990, ApJ 353, 469.
Lerche I., Schlickeiser, R. 1982a, MNRAS 201, 1041
Lerche I., Schlickeiser, R. 1982b, A&A 107, 148
Mirabel I. F. 1982, ApJ 256, 112.
Norman C., Ikeuchi, S. 1989, ApJ 345, 372.
Normandeau M., Taylor A. R., Dewdney, P. E. 1996, Nat 380, 687.
Pohl M., Schlickeiser R. 1990a, A&A 234, 147
Pohl M., Schlickeiser R. 1990b, A&A 239, 424
Rand R. J., van der Hulst, J. M. 1993 AJ 105, 2098.
Reich P., Reich, W. 1988, A&A 196, 211.
Reuter H.P., Klein U., Lesch H., Wielibinski R., Kronberg, P.P. 1995, A&A 293, 287
Seaquist E.R., Odegard, N. 1991, in *The Interpretation of Modern Synthesis Observations of Spiral Galaxies*, eds N. Duric and P.C. Crane, ASP Conference Series 18, 67
Shapiro P. R., Field G. B. 1976, ApJ 205, 762.
Stephens S.A. 1991, in *The Interstellar Disk-Halo Connection in Galaxies*, ed. H. Bloemen, p. 323.
Sukumar S., Velusamy T., Klein, U. 1988, MNRAS 231, 765.
Taylor J.H., Cordes, J. M. 1997, Preprint (Submitted to ApJ).
Veilleux S., Cecil G., Bland-Hawthorn, J. 1995, ApJ 445, 152.
Wentzel D.G. 1974, ARA& A 12, 71.

This article was processed by the author using Springer-Verlag LaTeX A&A style file *L-AA* version 3.